Molecular Dynamics Simulation in Nanoscale Heat Transfer: A review

D. Poulikakos, S. Arcidiacono

Laboratory of Thermodynamics in Emerging Technologies, Institute of Energy Technology,

Department of Mechanical and Process Engineering, Swiss Federal Institute of Technology, ETH

Center, CH-8092, Zurich Switzerland, dimos.poulikakos@ethz.ch, www.ltnt.ethz.ch

and

Shigeo Maruyama

Department of Mechanical Engineering, The University of Tokyo, 7-3-1 Hongo, Bunkyo-ku,

Tokyo 113-8656, Japan, maruyama@photon.t.u-tokyo.ac.jp, www.photon.t.u-tokyo.ac.jp

1. INTRODUCTORY COMMENTS

A promising approach to investigate nanoscale phenomena (including nanoscale heat transfer) is Molecular Dynamics (MD) simulation. In this approach, one works directly at the molecular (resp. atomic) level. By solving Newton's equation of motion of every molecule in the system of interest numerically, detailed information on the entire nanoscopic (hopefully in the not too distant future also microscopic) system can be obtained. Although this idea is not new (it dates back to the 1950s and 1960s, when pioneering investigations were performed in the field of theoretical physics), it is not until recently that its employment in relatively "large" systems (involving several thousand particles or more) has begun. To exemplify, early studies, in 1957, Alder and Wainwright [1] focused on the dynamics of particles moving at constant velocity

between perfectly elastic collisions and in 1964, Rahman [2] successfully solved the equations of motion for a set of Lennard-Jones particles. In selected engineering systems, the MD method can provide information that allows the revision or verification of ad hoc assumptions of continuum theory. However, there are two formidable difficulties that need to be overcome: first, all relevant intermolecular interactions should be correctly accounted for, and second, a large number of molecules need to be simulated in order to bridge the gap between the molecular and the continuum levels and provide needed information for macroscopic models, or aid the understanding of the physics of the phenomena of interest. With the reference to the first difficulty mentioned above, physically correct potentials for the intermolecular interactions need to be available. Here one often relies on "ab-initio" calculations. Hence, although the molecular dynamics method deals with classical forces, the potentials necessary to determine these forces are often the result of quantum mechanical calculations. With reference to the second difficulty, it is hoped that the continuously and rapidly increasing computer speed, combined with constant improvements in the development of efficient computational algorithms, will allow for the realization of engineering computations that bridge the gap between the nano- and microscales, in other words, reach sizes after which continuum theory is applicable.

2. THE BASIC PRINCIPLE OF THE MOLECULAR DYNAMICS SIMULATION METHOD

The main premise of Molecular Dynamics simulation can be described as follows: considering the fact that at the primitive level every substance is made from elementary particles (atoms or molecules), if the basic dynamics parameters of these molecules, i.e. position, velocity, and interaction force, can be determined, the macroscopic physical properties of the substance,

like volume, temperature, pressure, etc. can subsequently be obtained with a “bottom up” approach, via statistical methods. Based on this idea, the starting point of MD is Newton’s second law. For the translational motion of a spherically symmetric molecule, this law has the simple form:

$$\boldsymbol{F} = m\,\frac{d^2\boldsymbol{r}}{dt^2} \qquad (1)$$

where F is the sum of the forces exerted on the molecule by the other molecules in the system,

$\boldsymbol{r}$ is the position vector of the molecule,

$\boldsymbol{t}$ is the time, and

$\boldsymbol{m}$ is the mass of the molecule

Integrating equation (1) once in time yields the velocity of the molecule. Integrating once more results in its displacement. If one integrates equation (1) for every molecule in the simulation domain step by step from some initial state, then detailed information of the movement of every molecule is obtained. This information can be further processed by time averaging, space averaging or both to provide the macroscopic physical properties over the entire simulation domain.

For molecules that have internal complex geometry, the original simple Newton equation of motion is no longer sufficient. Depending on the type of molecular model used, a generalized form of the original Newton equation is adopted in the simulations. For example, using a rigid-body model, one has to consider the rotation of the molecule around its mass center; therefore the so-called "Euler Equation" should be used. However, no matter how complex the form of the equation of motion, the basic simulation procedure is always the same: first,

integrating the equation of motion of every molecule to acquire its dynamical parameters; then performing an averaging of these dynamical parameters to obtain the values of macroscopic physical properties.

As discussed earlier, one of the core problems (resp. difficulties) in Molecular Dynamics is the form and magnitude of the force term in the left-hand side of eq. (1). To calculate the interaction force among molecules, since in nature this force is electric/electromagnetic, one needs to have available an appropriate corresponding intermolecular potential model. Usually, this model comes from experimental data or quantum mechanics calculations (as mentioned earlier) and accounts for the contribution from two-body and three-body potentials. For calculations in a group of molecules, a many-body potential needs to be used [3]. Due to their small contribution to the total potential (and their significant impact on computational speed) the effect of more than two or three bodies in the potential equation is either overlooked, when acceptable from an accuracy standpoint, or simply appears as a correction term in the potential equation that can be calculated easily [4]. In many practical simulations, researchers consider only two-body potential so as to shorten the computational time with acceptable accuracy. Normally this is done by defining an "effective pair potential" and incorporating the effect of a three-body potential into this effective pair potential [4].

When a two-body potential model is chosen, the interaction force between a pair of molecules can be derived from this potential by the following relation:

$$\boldsymbol{F}_{ij} = -\nabla u_{ij} \tag{2}$$

where $\boldsymbol{F}_{ij}$ is the force acting on the i-th molecule by the j-th molecule, u_{ij} is two-body potential between the i-th molecule and the j-th molecule.

Summing up all the forces exerted on one molecule by other molecules yields the total

force on this molecule. After the total force on every molecule in the simulation domain has been calculated, one can integrate eq. (1) in time for each molecule.

Examples of potential functions for a host of materials relevant to heat transfer calculations are discussed in detail in a review paper by Maruyama [5] and will not be presented here for brevity. It will suffice to mention the popular for its simplicity but limited Lennard-Jones (LJ) 12-6 potential which assumes that the molecules are spherically symmetric

$$u(r) = 4\varepsilon\left[\left\{\left(\frac{\sigma}{r}\right)^{12} - \left(\frac{\sigma}{r}\right)^{6}\right\}\right] \tag{3}$$

where σ [m] and ε [J] are scales for length and energy, respectively. Depending on the type of molecules, appropriate values of the characteristic length and energy scales should be used in the LJ model. The variation of the potential with the molecular separation distance r implies that to bring two molecules from far apart into closer proximity, we must remove energy. Conversely, if two molecules are close enough to feel attractive forces, but not so close that repulsive forces come into play, then energy must be supplied to increase the spacing of the molecules.

A generalization and improvement of the Lennard Jones potential with similar limitations is the Stoddard & Ford potential [6], which features a shift for the continuous decay

$$u(r) = 4\varepsilon\left[\left\{\left(\frac{\sigma}{r}\right)^{12} - \left(\frac{\sigma}{r}\right)^{6}\right\} + \left\{6\left(\frac{\sigma}{r_c}\right)^{12} - 3\left(\frac{\sigma}{r_c}\right)^{6}\right\}\left(\frac{r}{r_c}\right)^{2} - \left\{7\left(\frac{\sigma}{r_c}\right)^{12} - \left(\frac{\sigma}{r_c}\right)^{6}\right\}\right] \tag{4}$$

The cut-off distance from the center of a spherical molecule or atom beyond which the effect of this potential is practically negligible is denoted by r_c. Again, more complex molecules are non spherical in nature and require more complex potentials. One such molecule very relevant to a many heat transfer applications is water. A review of potentials for water can be found in [5].

3. MOLECULAR DYNAMICS IN HEAT TRANSFER

Molecular level phenomena and their investigation are becoming with a very high rate important in heat and mass transfer research, driven both by the need to understand certain fundamental phenomena as well as by a plethora of new and forthcoming applications in the areas of micro- and nanotechnologies.

More specifically, studies of basic mechanisms of heat transfer such as in phase change demand the understanding of liquid-solid contact phenomena (such as wetting and nucleation) at the nanoscale level. Heat transfer in three-phase lines (evaporation or condensation of liquid on a solid surface, or solidification of a molten droplet on a surface) is a singular problem at the macroscopic level. The nucleation theory of a liquid droplet in vapor or of a vapor bubble in a liquid sometimes needs to take into account nuclei of the size of molecular clusters. The effect of the surfactant on the heat and mass transfer through liquid-vapor interface is also an example of the direct effect of molecular scale phenomena on the macroscopic problem. Even though much effort has been expended in extending macroscopic analyses to microscopic conditions in space (micrometer scale down to nanometer scale), time (microsecond, nanosecond and picosecond scales), and rate (extremely high heat fluxes of the order of Gigawatts), there is a clear limitation to these extrapolations. On the other hand, the development of the molecular dynamics (MD) computer simulation technique has demonstrated the possibility of tackling such phenomena from the opposite direction, by following a bottom up approach. The MD methods have long been used and are well developed as tools in statistical mechanics and chemistry [4, 7]. However, it is a new challenge to employ the method to the spatial and temporal scale of microscopic heat transfer phenomena and systems [5, 8]. At the same time, a host of novel technologies such as, the thin film manufacturing developed in the semiconductor industry, nanotube manufacturing and characterization, and the development of novel materials, demand the prediction of heat transfer

characteristics at the nanometer scale [9].

Two areas generic to many engineering applications where marked advances in molecular dynamics have already been made are phase change processes (at both ends, vaporization/condensation and freezing/melting) and heat conduction (exemplified by the determination of thermophysical properties of thin films). In the following, representative studies published in the open literature particularly in these areas will be reviewed, focusing on recent studies beyond the ones discussed in a recent review chapter by Maruyama [5].

3.1 Liquid-Vapor Interface

Surface tension is one of the benchmark properties to examine the applicability of the molecular dynamics method to a liquid-vapor interface and to evaluate the potential function model [5]. The typical simulation system is the liquid slab between vapor regions. When the liquid layer is thick enough, the bulk property of liquid can be obtained at the central region, and two liquid-vapor interfaces can be realized. By taking a time average, the density profile, pressure tensor, and surface tension can be reasonably predicted. The quite accurate prediction of surface tension has been demonstrated for Lennard-Jones fluid [10] and water [11] by integrating the difference of normal and tangential components of pressure tensor across the surface. The other typical configuration is the liquid droplet surrounded by its vapor [5, 12, 13]. When the size of the droplet is large enough, the bulk property of liquid is expected at the central region. The well-known Young-Laplace equation relates the curvature of a liquid-vapor interface and surface tension to the pressure difference. Thompson *et al.* [12] used the spherical extension of Irving-Kirkwood's formula to calculate the normal pressure profile. The definition of the radius of a droplet is not straightforward, since the size of the droplet is normally very small and the

liquid-vapor interface has a certain width. The equimolar dividing radius is one of the choices but more elaborate discussions based on statistical mechanics are found in the literature (see references in [5]). Roughly a thousand molecules are enough to calculate a reasonable value for the bulk surface tension for argon. At the other extreme, the surface tension for very small clusters, which may be important in nucleation theory, requires a completely different approach, because such a small cluster does not have the well-defined central liquid part assumed in the statistical mechanical discussions.

With reference to droplet vaporization, Long et al. [14] and Little [15] studied the evaporation of a liquid argon droplet exposed to both subcritical and supercritical surroundings using 5600 atoms, 27000 atoms and 100,000 atoms. The evaporation rate obtained by molecular dynamics simulation agreed well with existing theoretical results.

In recent publications, Walther *et al.* [16] and Walther and Koumoutsakos [17] investigated further the problem of subcritical evaporation of a nanometer-size droplet at 300 K and 3 MPa. Classical molecular dynamics techniques were combined with an adaptive tree data structure for the construction of the neighbor lists, allowing efficient simulations using hundreds of thousands of molecules. These high resolution simulations compute values of the evaporation coefficient that are in excellent agreement with theoretical predictions.

The determination of the condensation coefficient by MD simulations is also a challenging task. The condensation coefficient is simply defined as the ratio of rates of the number of condensing molecules to incident molecules. Through the detailed studies of the liquid-vapor inter-phase phenomena of argon, water, and methanol, Matsumoto et al. [18, 19] pointed out that this macroscopic concept could not be directly converted to the molecular scale and that the ‘molecular exchange’ process must be considered. On the other hand, Tsuruta et al.

[20] has reported a significant dependence of the trapping rate on the normal velocity of incident molecules.

Figure 1 shows the effect of surfactant in a liquid-vapor interface. Daiguji [21] simulated the effect of n-alcohols in the liquid-vapor interface of water or LiBr-water solution. Here, three n-alcohols with different hydro-carbon chain length (n-propanol, C_3H_7OH; n-heptanol, $C_7H_{15}OH$; and n-undecanol, $C_{11}H_{23}OH$) were modeled with OPLS potential [22] and water was modeled with the popular SPC/E potential [23]. Only for the moderate length alcohol, n-heptanol, the instability of the interface was observed for certain concentration as shown in Figure 1. When the alcohol concentration was lower as in Figure 1 (a), a monolayer of alcohol molecules with its hydrophilic site heading to water was stable. On the other hand, the 2-layers of alcohol molecules could be stable with the hydrophilic and hydrophobic interaction of 2-layers as in Figure 1 (c). With the medium concentration in Figure 1 (b), it seems that the alcohol molecules seek for more hydrophilic interaction with water molecules by creating the disturbance in the surface. Daiguji [21] further analyzed these phenomena from the thermodynamics standpoint and addressed the connection to the onset of Marangoni instability.

Arcidiacono *et al.* [24] studied the behavior of oscillating nanodroplets with around 320,000 argon atoms. The equilibrated droplet was "squeezed" with an imposed velocity field and, subsequently, it was allowed to oscillate freely. The oscillation frequency and the damping constant describing the time transient of the oscillation were in agreement with the macroscopic theory within 20%.

3.2 SOLID-LIQUID-VAPOR INTERACTIONS

Solid-liquid-vapor interaction phenomena play an important role in phase-change heat

transfer. The importance of the liquid wettability to the surface is apparent in dropwise condensation, high-heat-flux boiling heat transfer and capillary liquid film evaporators. There are good reviews of the connection between microscopic and macroscopic views of the wetting phenomena by Dussan [25], and from a more microscopic point of view by Koplik and Banavar [26]. Furthermore, the MD treatment of a simple Lennard-Jones liquid droplet on a solid surface and a Lennard-Jones vapor bubble on a solid surface are discussed in [5]. In brief, except for a few layers of atoms near the surface, the averaged shape of the Lennard-Jones liquid droplet is close to semi-spherical. By fitting a circle to the density contour disregarding the two layers of liquid near the solid surface, a "contact angle" can be measured. Controversially enough, the cosine of the measured contact angle is linearly dependent on the strength of the surface potential. The controversial discussions whether Young's equation can hold or not in such system has been historically discussed [5].

As the more practical example of solid-liquid-vapor interaction, a water droplet on a platinum solid surface is shown in Figure 2 [27]. Water molecules were modeled with the SPC/E potential [23] and the interaction potential between water and platinum molecules was expressed by the potential function developed by Zhu and Philpott [28], based on the extended Hückel calculations. The contact structure of the water droplet with a finite contact angle on the absorbed monolayer water film is realized for the first time with molecular dynamics simulation. The contact angle is determined by the surface energy between this monolayer water film and bulk liquid water. This monolayer film has quite high density due to the strong interaction to the platinum surface atoms. The interaction of this water film with normal water strongly depends on the density of the film. Higher density of water monolayer results the lower interaction. Hence, the dependence of contact angle on the platinum crystal lattice structure is explained by the

structure of this monolayer water film.

The behavior of carbon nanotubes (CNT) in a water environment is needed in order to understand the possibility of using CNT as nanofluidic devices. Some recent experimental works [29, 30] studied CNT synthesized by a hydrothermal method, in which some aqueous fluid was entrapped inside (Figure 3). As showed in the picture, the two menisci in the liquid-vapor interface indicate that the fluid wets the carbon nanotube wall. Another experimental work [31] suggest that liquids with a surface tension lower than 100-200 mNm^{-1} can wet CNT, *i.e.* is expected that water, with a surface tension of 73 mNm^{-1}, should wet CNT. Walther *et al*. [32-34] studied extensively the phenomenon via classical molecular dynamics. The CNT was simulated by Morse stretch, harmonic bend, torsion and LJ potential, the water with the SPC model and the interaction water-CNT with LJ potential describing the van der Waals interaction between oxygen and carbon. A quadrupole interaction between the carbon and the partial charges on hydrogen and oxygen atoms was also considered. In the mentioned works the authors investigated both CNT in water environment and water droplets inside a CNT. They found that pure water does not wet CNT. On the contrary, the nanotube was strongly hydrophobic (Figure 4). The water molecules are almost oriented parallel to the CNT surface and stand off from the nanotube at a distance of a few some angstroms. The number of hydrogen bonds decreases in the proximity of the nanotube. They evaluated the energy balance related to the insertion of a nanotube in water. The process results to be endoenergetic and the main contribution in energy is related to the work done to create a cavity where access the nanotube. The evaluated contact angle was around 105° (near the macroscopic value of about 80°÷90° for the contact angle water-graphite) and small variations were induced when the interaction constant between water and CNT was changed of ±20%. The large difference with the experimental results can be due

(speculatively) to the different behavior of pure water compared with the aqueous solution present in the CTN studied in [29, 30].

The coating of a substrate with a thin film has important applications in new technologies. In these processes the stability of the film, that is whether the film remains uniformly distributed or a dewetting phenomenon occurs, has a crucial role. The instability of the film is caused by a competition between the surface tension and van der Waals forces, acting between liquid and solid atoms, and is bigger in thinner films. Figure 5 shows the rupture of a thin film on a plate [35]. The rupture evolves with an approximate circular shape as predicted by the macroscopic three-dimensional rupture theory. The rupture time and rupture velocity propagation are strictly related with the liquid-liquid and solid-liquid interaction parameters used in the LJ potential [35]. Larger liquid-liquid interactions correspond to a shorter rupture time and, on the contrary, the resistance to rupture becomes larger as the solid-liquid interaction becomes bigger. Liu *et al.* [36] found that for polymers there is a limit dry area after which the instability grows and dewetting takes place. Moreover they showed, both with numerical and some theoretical considerations, that for a non volatile fluid the time growth of the length of the dry patch goes with $t^{1/2}$. On the contrary Koplik and Banavar [37] affirm that each dry patch leads to the instability and the growth rate, evaluated from their simulations, goes roughly with $t^{1/4}$. The difference is probably due to the fact that Liu *et al.* [36] used a pure repulsive and unstructured substrate on which the liquid "slides". Figure 6 depicts the dewetting time evolution of the film [37]. The film forms a rim that grows as it moves, the contact angle is smaller than his static counterpart and there is no second contact angle where the rim meets the flat part of the film (on the left in the Figure).

Moseler and Landman [38] performed molecular dynamics simulations revealing the

formation and break up of nanojets with velocities up to 400m/s. The jet generation was created with pressurization and injection of liquid propane from heated convergent gold nanonozzles. Heating was necessary to control condensation and subsequent wetting of the nozzle region around the nozzle. The atomistic description is very interestingly connected to continuum modeling with the derivation of a stochastic lubrication equation accounting for thermally triggered fluctuations. This paper has several unusual features for it combines phenomena having to do with droplet generation at the nanolevel, surface wetting and heat transfer, as well as theoretical explanations of the numerical findings by expanding on continuum concepts.

3.3 Nucleation and Phase Change

Homogeneous nucleation is one of the typical macroscopically investigated phenomena directly affected by molecular scale physics. Recently, Yasuoka *et al.* have demonstrated direct MD simulations of the nucleation process for Lennard-Jones [39] and for water [40] molecules. The key technique for such a calculation is the temperature control as discussed by Ikeshoji et al. [41] by observing the magic number clusters of 13, 19 and 23, which are abundantly observed in experimental mass spectra. After quenching to the supersaturation condition, the condensation latent heat must be removed for the successive condensation. Yasuoka *et al.* [39] used 5,000 Lennard-Jones molecules for the simulation, mixed with 5,000 soft-core carrier gas molecules connected to the Nosé-Hoover thermostat for the cooling agent. This cooling method mimicked the carrier gas of supersonic jet experiments. Through the detailed study of growth and delay of nuclei size distribution, they have estimated the nucleation rate and the critical size of nucleus. The nucleation rate was seven orders of magnitude larger than the prediction of classical nucleation theory. Their similar simulation [40] for water of TIP4P potential at 350 K, resulted in a nucleation rate two orders of magnitude smaller than the classical nucleation theory, in good

agreement with the “pulse expansion chamber” experimental results.

Heterogeneous nucleation is also obviously important in many heat transfer problems. Figure 7 shows an example of heterogeneous nucleation of a liquid droplet on a solid surface [42]. Argon vapor consisting of 5760 Lennard-Jones molecules was suddenly cooled by the solid wall controlled with the phantom technique [5]. The phantom molecules modeled the infinitely wide bulk solid kept at a constant temperature with proper heat conduction characteristics. The potential between argon and solid molecules was also represented by the Lennard-Jones potential function, and the energy scale parameter was adjusted to reproduce various wettabilities. After the equilibrium condition at 160 K was obtained, the temperature of the solid surface was suddenly set to 100 K or 80 K by the phantom molecule method. Initially, small clusters appeared and disappeared randomly in space. Then larger clusters grew preferentially near the surface for wettable cases. On the other hand, for the less wettable condition, relatively large clusters grew without the help of surface just like in homogeneous nucleation. The nucleation rate and free energy needed for cluster formation were not much different than the prediction of the classical heterogeneous nucleation theory in the case of smaller cooling rate.

An MD simulation of homogeneous [43] or heterogeneous [44] nucleation of a vapor bubble is much more difficult compared to the nucleation of a liquid droplet. Even though the formation of a vapor bubble can be reproduced by expanding the liquid to the negative pressure, qualitative comparison of the nucleation rate or critical radius is not easy.

The intermediate cluster structures are extremely important when some of them can be stably observed as end products, such as in the simulation of fullerene formation [45, 46] and endohedral metallofullerene formation [47]. To exemplify, Figure 8 shows the nucleated cluster distributions observed in a simulation related to the single-walled carbon nanotube generation.

Using the simplified Brenner [48] potential for carbon-carbon interaction and the empirical metal-carbon potential functions [47], the growth of metal-carbon binary clusters from a completely random vapor mixture of 2500 carbon and 25 Ni atoms was simulated. As shown in the inserted expanded views in Figure 8, many relatively large clusters up to about 100 carbon atoms and a few metal atoms were observed. Even though careful annealing examinations are necessary for the compensation of the accelerated simulation, these cluster structures were qualitatively in good agreement with the FT-ICR experimental results [49].

Pan *et al.* [50] went beyond the nucleation problem and performed molecular dynamics simulations of the vaporization phenomenon of an ultra-thin layer (2 nm) of liquid argon on a Platinum surface. The simulation started from a molecular system of three phases (liquid Argon, solid Platinum and Argon vapor) at equilibrium at 110 K. The Platinum wall was then suddenly heated to a higher temperature (a moderately higher temperature of 150 K and a much higher temperature of 300 K were investigated). The entire vaporization process was successfully simulated. The results reveal trends that agree with our knowledge of vaporization of a similar macroscopic system. For example, for the high surface temperature (Figure 9) the vaporization process is reminiscent of the Leidenfrost phenomenon and after the formation of a vapor region between the surface and the liquid mass, the latter deforms and tends to approximately acquire a spherical “droplet” shape. Contrary to this, a gradual evaporation process occurs at moderate wall temperatures. After complete evaporation and upon reduction of the wall temperature, condensation takes place leading to reconstruction of the initial liquid layer.

Koplik *et al.* [51] studied the solidification, evaporation and coalescence, described in the next paragraph, of nanodroplets with up to $O(10^5)$ atoms. The fluid atoms were simulated using the LJ potential and a finitely extensible nonlinear elastic (FENE) force to link atoms into

chain molecules. Molecules of 2, 10 and 100 atoms were studied during solidification. The droplets formed by longer chains showed an amorphous structure; on the contrary the dimer molecule system had a local crystalline structure. No orientation of the molecules was noticed in all the simulations except near the substrate where there is the tendency of molecules to orient parallel to it. Presumably the solidification time was too short compared with that required for a molecular rearrangement. The simulation of droplet evaporation was done adjusting the parameters in eqn. (3), describing the interaction between solid and liquid, so that at the equilibrium the contact angle was 45°. During the evaporation there was a thickening of the interface region and the contact angle decreased to about 30° as predicted by a recent analytical work.

The deposition of a molten droplet spreading on a cold substrate, with a temperature below the solidification point, is a process involved in many industrial applications. Standard macroscopic models have difficulties to simulate the contact line behaviour in which there is a singularity in shear stress, the no-slip boundary condition can not be applied and *ad hoc* assumptions are needed. Some works investigated the spreading process of LJ or chain molecules [26, 52-56], showing controversial results. Finally, Bekink *et al.* [55] reported the same time dependence of the radii of the spreading layers with $t^{1/2}$, as expected from experiments.

Ge *et al.* [57] considered spreading of a Cu liquid droplet on a Cu surface with a temperature well below the melting point. The thermodynamic system was simulated using the embedded atom method (EAM), see [58] and references therein. The time dependence of the spreading index (defined as the ratio between the equivalent radius of the area of the first layer of atoms spreading and the initial radius of the droplet) agrees well with the experimental contact area radius as a function of time. They concluded that for a rapid solidification the no-slip

boundary condition for the contact line can still hold.

3.4 Coalescence

In many industrial processes it is important to predict the behavior of small droplets in sprays and aerosols. Continuum models based on the Navier-Stokes equations can reproduce the evolution of the droplet shape but still boundary conditions coming from first principles are missing and approximations have to be adopted. Molecular dynamics allows for the study of droplet phenomena from a molecular point of view accounting non-empirically for complicated boundary conditions, e.g. the presence of surfactants on the surface of the droplet. A review on coalescence and break up phenomena related to atomization and spray applications can be found in [59]. Typical findings of MD simulations are presented below.

When the two droplets are sufficiently close to one another (Figure 10) [60], some molecules, due to thermal fluctuations, can leave one droplet and move within the interaction range of the molecules of the other. These molecules start attracting others creating a thin filament joining the two drops. The resulting droplet shape has a high-enough surface energy to reduce thickening the filament and finally give a spherical shape to the drop. Figure 11 depicts the coalescence of a cylinder falling under a gravity force into a tank of molecules of the same liquid, in presence of an immiscible liquid (not showed in the figure) [60]. The coalescence mechanism is quite similar to that described above. Koplic and Banavar [51] extended the cited work to bigger droplets with a more complex potential to mimic chain molecules. The time dependence of the radius of the neck of the coalescing droplets was compared with the continuum theory but no agreement was found. The dynamics of coalescence was the same with that found for monoatomic molecules.

Lehtinen and Zachariah [61, 62] showed, in some MD simulation of Si droplets, that the

heat transfer and the initial boundary conditions in temperature play a crucial role in this phenomenon. When two particles coalesce new chemical bonds are formed with a resulting heat generation (Figure 12). Depending on the exchanged heat, the droplet temperature can increase leading a decrease in the coalescence time. They found that below a critical temperature of the surrounding gas, the heat generated is released to the gas and the temperature of the particle does not increase. Above the critical temperature, a sharp increase in the particle temperature is observed with a decrease in the coalescence time.

3.5 Other Topics Related to Nanotechnology Systems

As an example of a "nanotechnology system" investigated with molecular dynamics simulations, is hydrogen absorption by carbon nanotubes as shown in Figure 13 [63]. Assuming the physical adsorption of hydrogen to occur at the surface of carbon nanotubes, the potential forms between H_2-H_2 and C-H_2 were both expressed by Lennard-Jones (12-6) functions. Each nanotube was regarded as rigid and the van der Waals potential between the nanotubes was derived as a Lennard-Jones (8-4) function by integrating the potential between carbon atoms. During 500 ps simulation at 12 MPa and 77 K, the adsorption was observed only inside the tubes and outside the bundles. It was needed to once reduce the van der Waals potential between nanotubes to observe the phase transformation from the close packed bundle to the structure accommodating a hydrogen layer between the tubes as in Figure 13 (a). The phase transformation in the opposite direction was simulated by reducing the hydrogen pressure step as needed down to 6 MPa as shown in Figure 13 (b) and Figure 13 (c).

Since many direct heat transfer problems of nanotechnology are currently related with thermophysical properties of solid materials, the heat conduction behavior of micro- and nanodevices is of importance. For best design of micro and nanodevices the knowledge of the

dependence of thermal properties with temperature and dimension of the device is of interest.

Based on the phonon dynamics approach [64], the direct calculation of phonon relations, phonon mean free path, and phonon scattering rates using the molecular dynamics simulations are modeled [65,66].

The thermal conductivity of a solid can be predicted by standard MD when the heat conduction is dominated by phonons. Both non equilibrium MD (NEMD) and equilibrium MD (EMD) can be used (see [67] and reported references). The former uses a "direct method", a temperature gradient is imposed across the simulation domain, realizing an analogy to the experimental situation, and the conductivity is simply evaluated as the ratio between the imposed heat flux and temperature gradient. In the second approach, the thermal conductivity is calculated through the heat flux fluctuations via the fluctuation-dissipation theorem using the Green-Kubo correlation.

The evaluation of bulk conductivity is possible when the dimensions of the computational domain are bigger than the mean free path of the phonons. This can result in simulations with several hundred millions atoms over 10^6 time steps. To avoid this problem Volz and Chen [69], using the Green-Kubo correlation, found a correction that took into account the cut off to low frequency phonons induced by periodic boundary conditions. The obtained thermal conductivity for Si crystals was not size dependent. The same authors [70] studied the heat transfer and the thermal conductivity of Si/Ge superlattices showing that the MD approach can yield heat transfer properties overcoming the difficulties of the phonon transport theory.

It is experimentally known that the thermal conductivity of thin films is lower than its bulk counterpart. Lukes *et al.* [68] studied an argon-type thin film via NEMD. They confirmed this trend and found that the dependence on the film length can be more pronounced at lower

temperatures.

The result of a heat conduction MD simulation along a carbon nanotube is shown in Figure 14 [71, 72]. The potential function employed was the Tersoff-Brenner bond order potential [48]. The thermal conductivity of nanotubes, which was speculated to be higher than that of many conductive materials (including diamond) along the cylindrical axis, was obtained from simulations for nanotubes with several different chiralities and lengths. The temperature at each end of a nanotube was controlled by the phantom technique [5], and no periodic boundary condition was applied to minimize the boundary scattering of phonons.

The thermal conductivity was calculated from the calculated temperature gradient as shown in Figure 14 (a) and the heat flux was obtained by integration of the additional force by the phantom molecules. The preliminary results showed that the thermal conductivity was about 200 ~ 300 W/mK. The temperature jump near the heating and cooling region was explained by assuming a thermal boundary resistance due to the miss-match of the phantom technique and the structured phonon density distribution. The phonon dispersion relations were directly calculated as the time-space 2-D Fourier transform of the position of each molecule as shown in Figure 14 (b). The relation to the solid-solid thermal boundary resistance and more generally to the liquid-solid thermal boundary resistance [73] can be simulated. Ohara *et al.* have analyzed the possible explanation of this thermal boundary resistance [74] based on their "intermolecular energy transfer" concept developed by the detailed studies of heat conduction in liquid phase water [75] and a Lennard-Jones fluid [76].

Another interesting field in new industrial processes is the irradiation with short pulse lasers for the manufacture of surfaces. The final chemical and physical properties, due to the short pulse time, are difficult to investigate experimentally. Computer simulations can help to

understand the underlying physical phenomena related to the changing of the structure of the material and the laser pulse characteristics. Häkkinen and Landman [77] simulated the irradiation of fcc (100), (110) and (111) Cu atoms coupling the electron phonon absorption with the heating of the lattice. The EAM [58] potential was used to describe the metallic bond. For the same laser pulse, the (100) and (110) surfaces melt while the (111) lattice maintained the crystalline order and showed a superheating over the melting point. The high stability of the (111) was observed also for highly defective surfaces. In this case the superheating was coupled with the annealing of the surface structure through a non diffusive process that restored the crystalline structure.

Herrmann *et al.* [78] studied the ablation of silicon and compared the final structure obtained irradiating the surface with different energies and length of the laser pulse. They concluded that, using the same laser energy, shorter pulse lengths remove more material but this leads to a cylindrical ablation (the typical Gaussian shape is lost) and less deep holes. Surfaces irradiated with multishot lasers showed narrower and deeper holes compared with those done with only one shot of the same energy.

Wang and Xu [79] focused on heat transfer, melting and evaporation of argon during laser energy adsorption at different fluencies. The heat transfer during irradiation without phase change was compared to a finite difference simulation and good agreement was found, showing that even at this scale continuum approach is valid. The results of the simulation of the phase change predict some interesting phenomena. The solid-liquid interface is not sharp. A buffer zone is present, where liquid and solid coexist. The velocity of the liquid-solid interface is well below of the local sound speed. During the transient, superheating is observed both in the liquid-vapor interface and in the melting front. After the melting process stops, the temperature in the solid-liquid interface drops below the melting point corresponding to the imposed system

pressure.

SUMMARY

With emergence of new technologies a bigger attention is focused on heat transfer at small scales. High heat transfer, discontinuities in solid-liquid-vapor interface, slip in the flow in micro channels impose a limit to the usage of continuum approach.

These problems can be overcome with the MD approach, once a correct potential mimicking molecules interaction is found.

In the limit of computations with a large number of atoms, bulk properties and behavior of the studied systems are in good agreement with the macroscopic theory and experimental values. This aspect could allow extrapolating boundary conditions from first principles that could be used in macroscopic simulations such as, for example, slip length or a criterion to discern when coalescence takes place.

Unluckily the experiments are not always comparable with MD results and an assessment of the method is quite difficult. Moreover the classical MD approach can not simulate the conduction due to free electrons and heat transfer in metals is not easy to perform.

ACKNOWLEDGEMENTS

One of the authors (SM) thanks Professor H. Daiguji at the University of Tokyo for offering the original figure for this paper.

REFERENCES

1. Alder, B. J., Wainwright, T. E. , 1957 , “Phase transition of a hard sphere system,” *J. Chem. Phys.*, Vol.27, pp. 1208-1209.

2. Rahman, A., 1964, "Correlations in the motion of atoms in liquid argon," *Phys. Rev. A*, Vol. 136, A405.

3. Pfalzner, S., Gibbon, P., 1996, Many-body tree methods in physics, Cambridge University Press, New York.

4. Allen, M. P., Tildesley, D. J., 1997, Computer simulation of liquids, Clarendon Press, Oxford.

5. Maruyama, S., 2000, "Molecular Dynamics Method for Microscale Heat Transfer," *Advances in Numerical Heat Transfer*, vol. 2, ed. W. J. Minkowycz and E. M. Sparrow, Taylor & Francis, pp. 189-226.

6. Stoddard, S. D., Ford, J., 1973, "Numerical experiments on the stochastic behavior of a Lennard-Jones gas system", *Phys. Rev. A*, Vol.8, pp. 1504-1512.

7. Haile, J. M., 1992, Molecular Dynamics Simulation, Wiley, New York.

8. Ohara, T., 2000, "Molecular Dynamics Study in Microscale Thermophysical Engineering: Current Activities and Future in Japan," *Micro. Thermophys. Eng.*, Vol. 4, No. 4, pp. 213-221.

9. Majumdar, A., 2000, "Nanoengineering: Promises and Challenges," *Micro. Thermophys. Eng.*, Vol. 4, No. 2, pp. 77-82.

10. Nijmeijer, M. J. P., Bakker, A. F., Bruin, C. and Sikkenk, J. H. , 1988, "A Molecular Dynamics Simulation of the Lennard-Jones Liquid-Vapor Interface," *J. Chem. Phys*., vol. 89, no. 6, pp. 3789-3792.

11. Alejandre, J., Tildesley, D. J., and Chapela, G. A., 1995, "Molecular Dynamics Simulation of the Orthobaric Densities and Surface Tension of Water," *J. Chem. Phys*., vol. 102, no. 11, pp. 4574-4583.

12. Thompson, S.M., Gubbins, K.E., Walton, J.P.R.B., Chantry, R.A.R. and Rowlinson, J.S., 1984, "A Molecular Dynamics Study of Liquid Drops," *J. Chem. Phys*., vol. 81, no. 1, pp. 530-542.

13. Nijmeijer, M.J.P., Bruin C., van Woerkom, A.B., Bakker, A.F. and van Leeuwen, J.M.J., 1992,"Molecular Dynamics of the Surface Tension of a Drop," *J. Chem. Phys*., vol. 96, no. 1, pp. 565-576.

14. Long, L. N., Micci, M. M., and Wong, B. C., 1996, "Molecular dynamics simulations of droplet evaporation," *Comp. Phys. Commun.*, vol. 96, pp. 167-172.

15. Little, J. K., 1996, "Simulation of droplet evaporation in supercritical environments using parallel molecular dynamics," Ph.D Thesis, Department of Aerospace Engineering, The Pennsylvania State University.

16. Walther, J. H., Pan, Y., Poulikakos, D., Koumoutsakos, P., 1999, "Molecular Dynamics Simulation of Evaporation and Coalescence of Nano-Size Droplets," *ASME Journal of Heat Transfer*, Vol. 121, No. 3, Transfer Gallery.

17. Walther, J. H. and Koumoutsakos, P., 2001, "Molecular Dynamics Simulation of Nanodroplet Evaporation," *ASME Journal of Heat Transfer*, vol. 123, no. 4, pp. 741-748.

18. Yasuoka, K., Matsumoto, M. and Kataoka, Y., 1994, "Evaporation and Condensation at a Liquid Surface. I. Argon," *J. Chem. Phys.,* vol. 101, no. 9, pp. 7904-7911.

19. Matsumoto, M., Yasuoka, K. and Kataoka, Y., 1994, "Evaporation and Condensation at a Liquid Surface. II. Methanol," *J. Chem. Phys.*, vol. 101, no. 9, pp. 7911-7917.

20. Tsuruta, T., Tanaka, H., Tamashima, K. and Masuoka, T., 1997, "Condensation Coefficient and Interphase Mass Transfer," *International Symposium on Molecular and Microscale Heat Transfer in Materials Processing and Other Applications* (ed. I.

Tanasawa and S. Nishio), Begell House, New York, pp. International Center Heat Mass Transfer Symposium, Yokohama, pp. 229-240.

21. Daiguji, H., 2001, "Molecular dynamics study of n-alcohols adsorbed on an aqueous electrolyte solution," *J. Chem. Phys.*, vol. 115, no. 4, pp. 1538-1549.
22. Jorgensen, W. L., 1986, "Optimized Intermolecular Potential Functions for Liquid Alcohols," *J. Phys. Chem*., vol. 90, pp. 1276-1284.
23. Berendsen, H. J. C., Grigera, J. R. and Straatsma, T. P., 1987, "The Missing Term in Effective Pair Potentials," J. Phys. Chem., vol. 91, no. 24, pp.6269-6271.
24. Arcidiacono, S., Ventikos, Y. and Poulikakos, D., 2002, "Oscillatory behavior of nanodroplets," MECT-02 International Symposium On Micro/Nanoscale Energy Conversion And Transport, International Centre for Heat and Mass Transfer (ICHMT), Antalya, Turkey.
25. Dussan, V. E. B., 1979, "On the Spreading of Liquids on Solid Surfaces: Static and Dynamic Contact Lines," *Ann. Rev. Fluid Mech.*, vol. 11, pp. 371-400.
26. Koplik, J. and Banavar, J. R., 1995, "Continuum Deductions from Molecular Hydrodynamics," *Ann. Rev. Fluid Mech.*, vol. 27, pp. 257-292.
27. Kimura, T and Maruyama, S., 2002, "Molecular dynamics simulation of water droplet in contact with platinum surface," *Proc. 12th Int. Heat Transfer Conf*., Grenoble, pp. 537-542.
28. Zhu, S.-B., and Philpott, M. R., 1994, "Interaction of Water with Metal Surfaces", *J. Chem. Phys.*, vol. 100, no. 9, pp. 6961-6968.
29. Gototsi, Y., Libera, J.A., Güvenç-Yazicioglu, A.G. and Megaridis, C.M., 2001, "*In Situ* Multiphase fluid Experiments in Hydrothermal Carbon Nanotubes," *Appl. Phys. Lett.*,

vol.79, no 7, pp. 1021-1023

30. Megaridis, C.M., Güvenç-Yazicioglu, A.G., Libera, J.A. and Gototsi, Y., 2002, "Attoliter Fluid experiments in Individual Closed-End Carbon Nanotubes: Liquid Film and Fluid Interface Dynamics," *Phys. Fluids*, vol.14, no 2, L5-L8
31. Dujardin, E., Ebbesen, T.W., Hiura, H., Tanigaki, K., 1994, "Capillary and Wetting of Carbon Nanotubes," *Science*, vol. 265, pp. 1850-1852.
32. Walther, J.H., Jaffe, R., Halcioglou, T. and Koumoutsakos, P., 2001, "Carbon Nanotubes in water; Structural Characteristics and Energetics," *J. Phys. Chem. B*, vol.105, pp. 9980-9987.
33. Werder T., Walther J.H., Jaffe R.L., Halicioglu T., Noca F. And Koumoutsakos P., 2001, "Molecular Dynamics Simulation of Contact Angles of Water Droplets in Carbon Nanotubes," *NanoLetters*, vol. 1, no 12, pp. 697-702.
34. Walther J.H., Jaffe R.L., Kotsalie E., Werder T., Halicioglu T. and Koumoutsakos P., 2002, "Hydrophobic Hydration of C_{60} and Carbon Nanotubes in Water," *J. Chem. Phys.*, in press
35. Hwang, C.C., Hsieh, J.Y., Chang, K.H. and Liao, J.J., 1998, "A Study Rupture Process of Thin Liquid Films by a Molecular Dynamics Simulation," *Physica A*, vol. 256, pp. 333-341
36. Liu, H., Bhattacharya, A. and Chakrabarti, A., 1998, "Early Stages of Dewetting of Microscopically thin Polymer films: a Molecular Dynamics Study," *J. Chem. Phys.*, vol. 109, no 19, pp. 8607-8611
37. Koplik, J. and Banavar, J.R., 2000, "Molecular Simulation of Dewetting," *Phys. Rev. Lett.*, vol. 84, no 19, pp. 4401-4404

38. Moseler, M. and Landman, U., 2000, “Formation, Stability and Break Up of Nanojets,” *Science*, Vol. 289, pp. 1165-1169.

39. Yasuoka, K. and Matsumoto, M., 1998, “Molecular Dynamics of Homogeneous Nucleation in the Vapor Phase. I. Lennard-Jones Fluid,” *J. Chem. Phys*., vol. 109, no. 19, pp. 8451-8462.

40. Yasuoka, K. and Matsumoto, M., 1998, “Molecular Dynamics of Homogeneous Nucleation in the Vapor Phase. II. Water,” *J. Chem. Phys*., vol. 109, no. 19, pp. 8463-8470.

41. Ikeshoji, T., Hafskjold, B., Hashi, Y. and Kawazoe, Y., 1996, “Molecular Dynamics Simulation for the Formation of Magic-Number Clusters with the Lennard-Jones Potential,” *Phys. Rev. Lett.*, vol. 76, no. 11, pp. 1792-1795.

42. Kimura, T. and Maruyama, S., 2002, "A Molecular Dynamics Simulation of Heterogeneous Nucleation of a Liquid Droplet on Solid Surface," *Micro. Thermophys. Eng.*, vol. 6, no. 1, pp. 3-13.

43. Kinjo, T. and Matsumoto, M., 1998, “Cavitation Processes and Negative Pressure,” *Fluid Phase Equilibria*, 144, pp. 343-350.

44. Maruyama, S. and Kimura, T., 2000, “A Molecular Dynamics Simulation of a Bubble Nucleation on Solid Surface,” Int. J. Heat & Technology, vol. 8, no. 1, pp. 69-74.

45. Yamaguchi, Y. and Maruyama, S., 1998, “A Molecular Dynamics Simulation of the Fullerene Formation Process,” *Chem. Phys. Lett.*, vol. 286-3,4, pp. 336-342.

46. Maruyama, S. and Yamaguchi, Y., 1998, “A Molecular Dynamics Demonstration of Annealing to a Perfect C_{60} Structure,” *Chem. Phys. Lett.*, vol. 286-3, 4, pp. 343-349.

47. Yamaguchi, Y. and Maruyama, S., 1999, “A Molecular Dynamics Study on the

Formation of Metallofullerene," The European Physical Journal D, vol. 9, no. 1-4, pp. 385-388.

48. Brenner, D. W., 1990, "Empirical Potential for Hydrocarbons for Use in Simulating the Chemical Vapor Deposition of Diamond Films," *Phys. Rev. B*, vol. 42, pp.9458-9471.
49. Maruyama, S., Kohno, M. and Inoue, S., 2000, "Chemical Reaction of Metal-Carbon Binary Cluster Anions by FT-ICR Mass Spectrometer," Fullerene 2000: Chemistry and Physics of Fullerenes and Carbon Nanomaterials, pp. 309-319.
50. Pan, Y., Poulikakos, D., Walther, J.H. and Yadigaroglou, G., 2002, "Molecular Dynamics Simulation of Vaporazation of an Ultra-Thin Liquid Argon Layer on a Surface," *Intl. J. Heat and Mass Transfer*, Vol. 45, pp. 2087-2100.
51. Koplik, J., Pal, S. and Banavar, J.R., 2002, "Dynamics of Nanoscale Droplets," *Phys. Rev. E*, vol. 65, 021504.
52. Yang, J., Koplik, J. and Banavar, J.R., 1991, "Molecular Dynamics of Drop Spreading on a Solid Surface", *Phys. Rev. Lett.*, vol. 67, no 25, pp. 3539-3542.
53. Nieminen, J.A., Abraham, D.B., Karttunen, M. and Kaski, K., 1992, "Molecular Dynamics of Microscopic Droplet on Solid Surface", *Phys. Rev. Lett.*, vol. 69, no 1, pp. 124-127.
54. Yang, J., Koplik, J. and Banavar, J.R., 1992, "Terraced Spreading of Simple Liquids on Solid Surfaces", *Phys. Rev. A*, vol. 46, no 12, pp. 7738-7749.
55. Bekink, S., Karaborni, S., Verbist, G. and Esselink K., 1996, "Simulating the Spreading of a Drop in the Terraced Wetting Regime", *Phys. Rev. Lett.*, vol. 76, no 20, pp. 3766-3769.
56. De Coninck, J., D'Ortona, U., Koplik, J. and Banavar, J.R., "Terraced Spreading of Chain

Molecules via Molecular Dynamics", *Phys. Rev. Lett.*, vol. 74, no 6, pp. 928-931.

57. Ge, R., Clapp, P.C., Rifkin, J.A., 1999, "Molecular Dynamics of a molten Cu Droplet Spreading on a Cold Cu Substrate," *Surf. Sci.*, vol. 426 (1), L413-L419.
58. Daw, M.S., Foiles, S.M. and Baskes M.I., 1993, "The Embedded-Atom Method: a Review of Theory and Applications," *Mater. Sci. Rep.*, vol. 9, pp. 251-310.
59. Micci, M.M., Kaltz, L.T. and Long, L.N., 2001, "Molecular Dynamics Simulations of Atomization and Spray Phenomena," *Atomization Spray,* vol.11, pp. 351-363
60. Koplik, J. and Banavar, J.R., 1992, "Molecular Structure of the Coalescence of Liquid Interfaces," *Science*, vol. 257, pp.1664-1666
61. Zachariah, M. R. and Carrier, M.J., 1999, "Molecular Dynamics Computation of Nanoparticle Sintering: Comparison with Phenomenological Models," *J. Aeros. Sci.,* vol. 30, pp. 1139-1151.
62. Lehtinen, K.E.J. and Zachariah, M.R., 2001, "Effect of Coalescence Energy Release on the Temporal Shape Evolution of Nanoparticles," *Phys. Rev. B*, vol.63, 205402.
63. Maruyama, S. and Kimura, T., 2000, "Molecular Dynamics Simulation of Hydrogen Storage in Single-Walled Carbon Nanotubes," Proc. ASME Heat Transfer Division 2000, Orlando, vol. 2, pp. 405-409.
64. Chen, G., 1998, "Thermal conductivity and ballistic-phonon transport in the cross-plane direction of superlattices," Phys. Rev. B, vol. 57, no. 23, pp. 14958-14973.
65. Tien, C. L., Lukes, J. R. and Chou, F.-C., 1998, "Molecular Dynamics Simulation of Thermal Transport in Solids," Microscale Thermophysical Engineering, vol. 2, no. 3, pp. 133-137.
66. Matsumoto, M., Komiyama, M., Makino, T. and Wakabayashi, H., 2000, "MD

Simulation and Phonon Analysis for Heat Conduction in Solids," Proceedings of the 37th Japan Heat Transfer Conference, vol. 3, pp. 975-976.

67. Schelling, K.P., Phillpot, S.R. and Keblinski, P., 2002, "Comparison of Atomic-Level Simulation Methods for Computing Thermal Conductivity," *Phys. Rev. B*, vol. 65, 144306

68. Lukes, J.R., Li, D.Y., Liang, X.G. and Tien, C.L., 2000, "Molecular Dynamics Study of Solid Thin-Film Thermal Conductivity," *J. Heat Trans.-T. ASME*, vol. 122, pp. 536-543

69. Volz, S.G., Chen, G., 2000, "Molecular-Dynamics Simulation of Thermal Conductivity of Silicon Crystals," *Phys. Rev. B*, vol. 61, no 4, pp. 2651-2656

70. Volz, S., Saulnier, J.B., Chen, G. and Beauchamp, P., 2000, "Molecular Dynamics of Heat Transfer in Si/Ge Superlattices," *High Temp.-High Press.*, vol. 32, pp.709-714.

71. Maruyama, S., 2002, "A Molecular Dynamics Simulation of Heat Conduction of a Finite Length Single-Walled Carbon Nanotube," *Micro. Thermophys. Eng.*, in press.

72. Maruyama, S., 2002, "A Molecular Dynamics Simulation of Heat Conduction of Finite Length SWNTs," *Physica B*, vol. 323, no. 1-4, pp. 193-195.

73. Maruyama, S. and Kimura, T., 1999, "A Study on Thermal Resistance over a Solid-Liquid Interface by the Molecular Dynamics Method," *Thermal Sci. Eng.*, vol. 7, no. 1, pp. 63-68.

74. Ohara, T. and Suzuki, D., 2000, "Intermolecular Energy Transfer at a Solid-Liquid Interface," Microscale Thermophysical Engineering, vol. 4, No. 3, pp. 189-196.

75. Ohara, T., 1999, "Intermolecular Energy Transfer in Liquid Water and Its Contribution to Heat Conduction: A Molecular Dynamics Study," *J. Chem. Phys.*, vol. 111, pp. 6492-6500.

76. Ohara, T., 1999, “Contribution of Intermolecular Energy Transfer to Heat Conduction in a Simple Liquid,” *J. Chem. Phys.*, vol. 111, pp. 9667-9672.

77. Häkkinen, H. and Landman U., 1993, “Superheating, Melting and Annealing of Copper Surfaces,” *Phys. Rev. Lett.*, vol. 71, no 7, pp. 1023-1026.

78. Herrmann, R.F.W., Gerlach, J. and Campbell E.E.B., 1998, “Ultrashort Pulse Laser Ablation of Silicon: an MD Simulation Study,” *Appl. Phys. A*, vol. 66, pp. 35-42.

79. Wang, X. and Xu, X., “Molecular Dynamics Simulation of Heat Transfer and Phase Change During Laser Material Interaction,” *ASME Journal of Heat Transfer.*, vol. 124, pp. 265-274

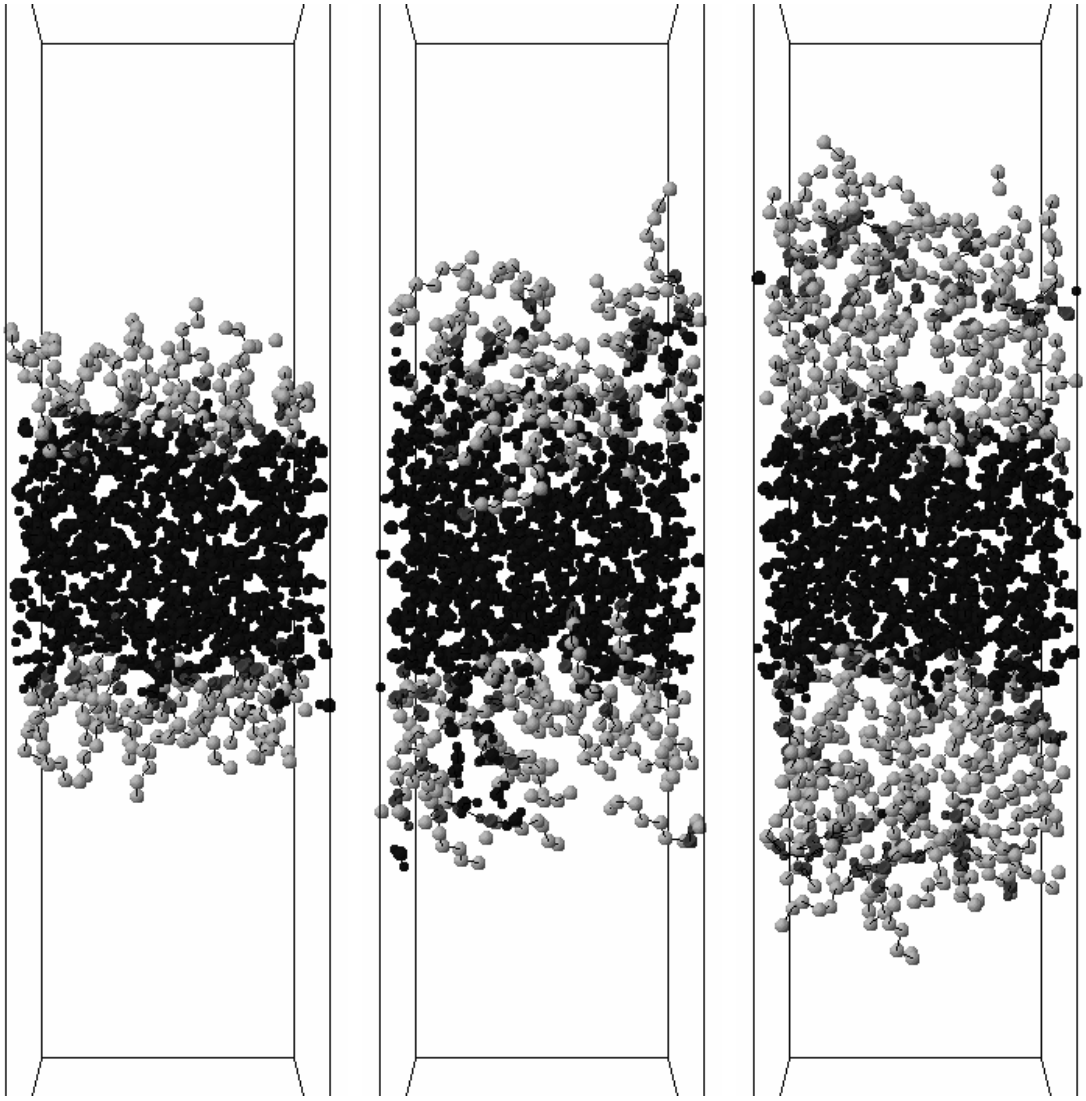

(a) $N_1 = 40$ (b) $N_1 = 60$ (c) $N_1 = 100$

Figure 1. Snapshots of n-heptanol and water mixtures as the function of number of n-heptanol molecules, [21]. The Number of water molecules N_2 is 400. The dark molecules in the middle are water. Note the instability of water-alcohol interface is observed only at the medium concentration in (b).

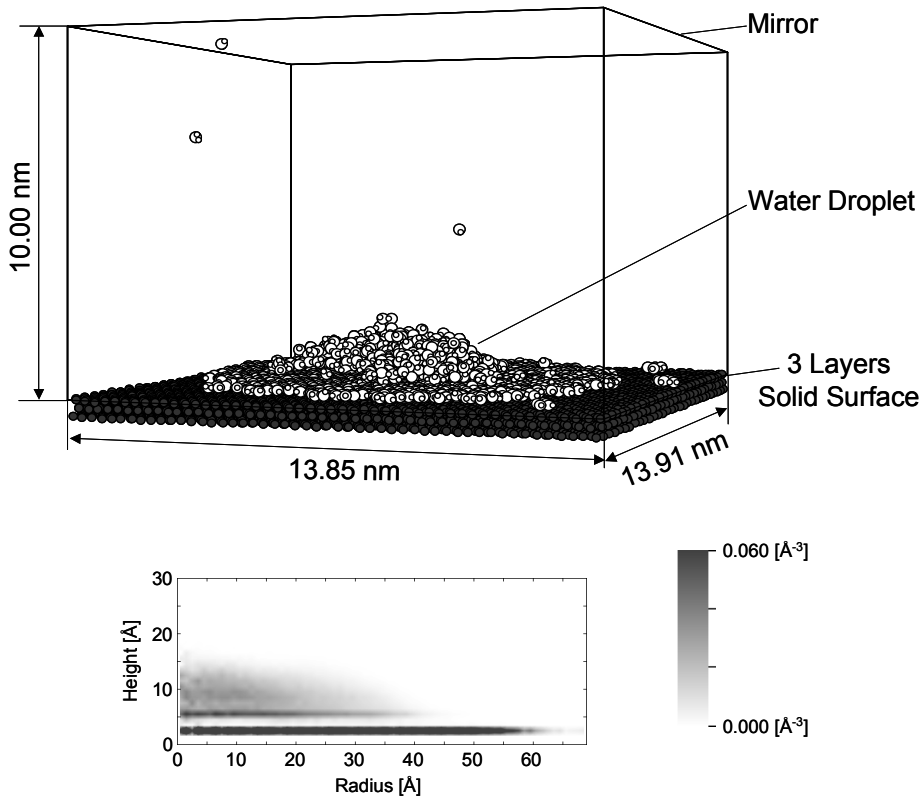

Figure 2. A snapshot and 2-dimensional density profile of an equilibrium water droplet on a platinum surface at 350K [27]. SPC/E water molecules were interacting with the harmonic platinum surface represented by 3 layers of (111) surface through the water-platinum potential proposed by Zhu-Philpott [28].

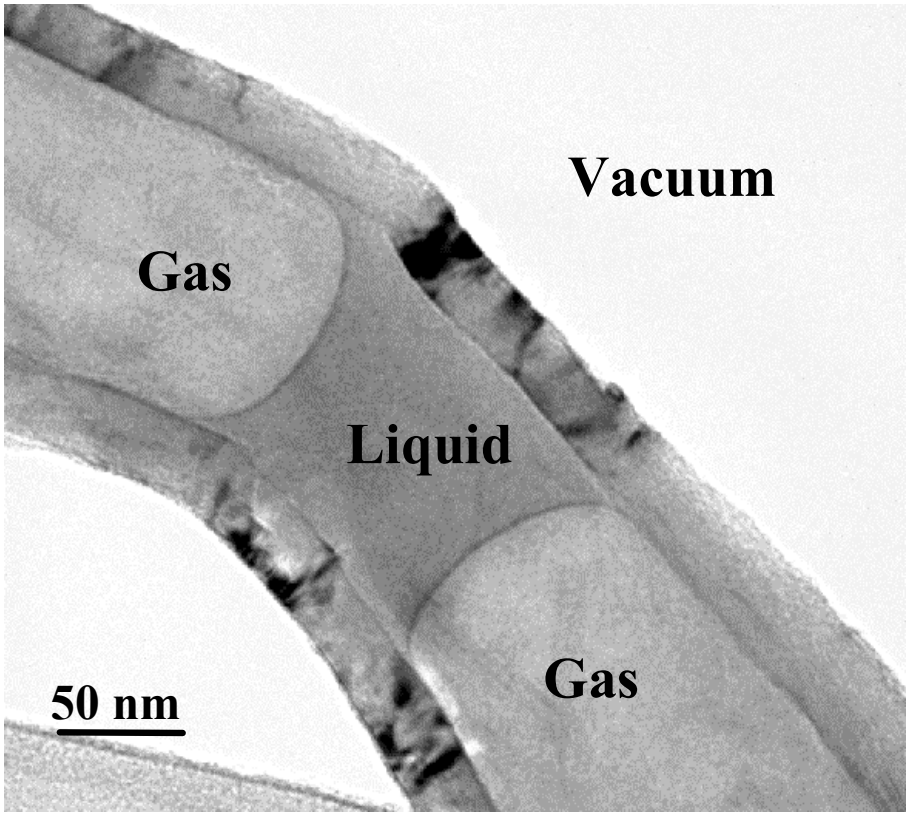

Figure 3. Transmission Emission Microscope image of liquid inclusion inside a carbon nanotube.

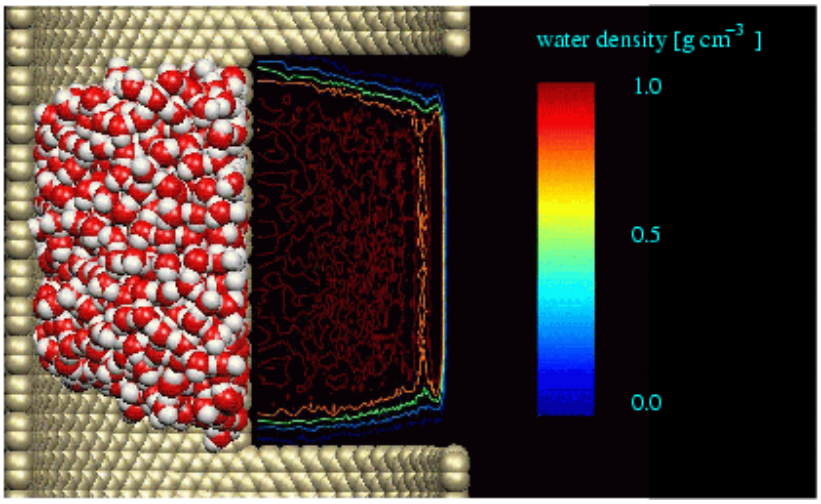

Figure 4. Water density distribution inside a carbon nanotube and contact angle evaluation [33].

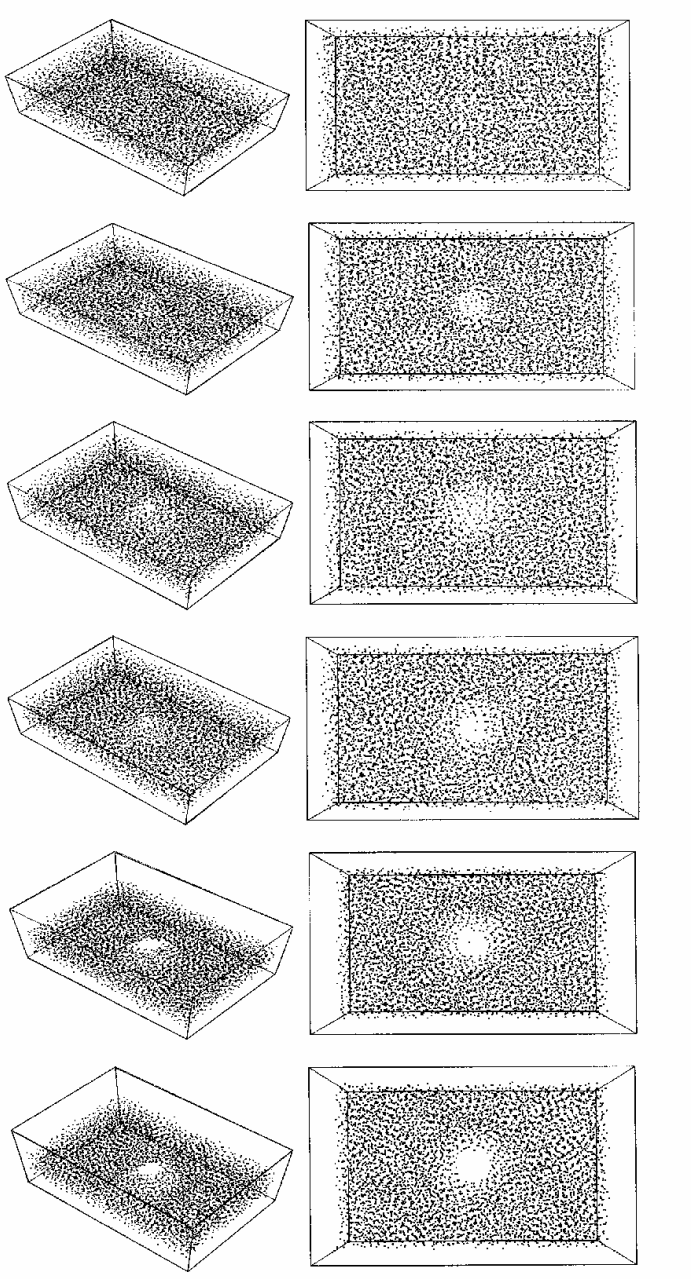

Figure 5. Time evolution of rupture of a thin film on a substrate, [35].

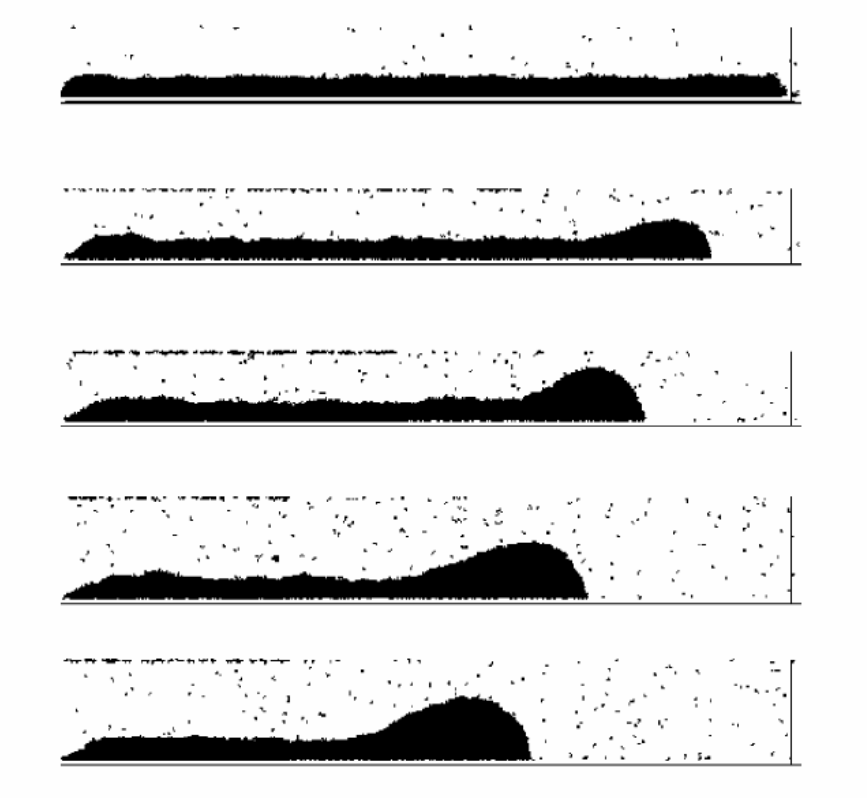

Figure 6. Time evolution of a dewetting film, [37].

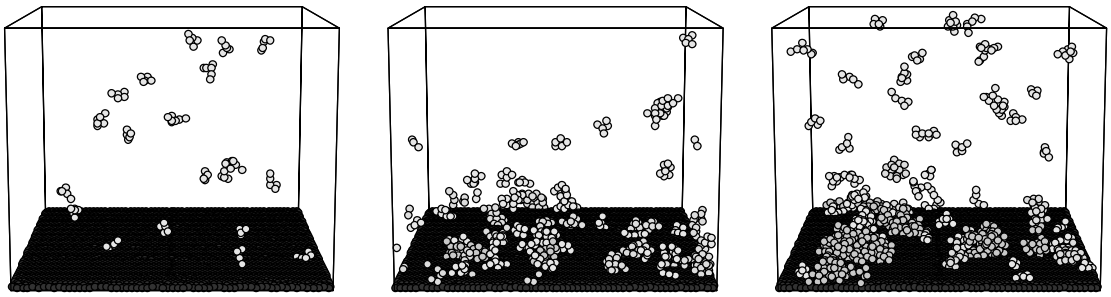

(a) 500 ps (b) 1000 ps (c) 1500 ps

Figure 7. Growth of liquid droplet clusters larger than 5 atoms by suddenly cooling the solid surface, [42].

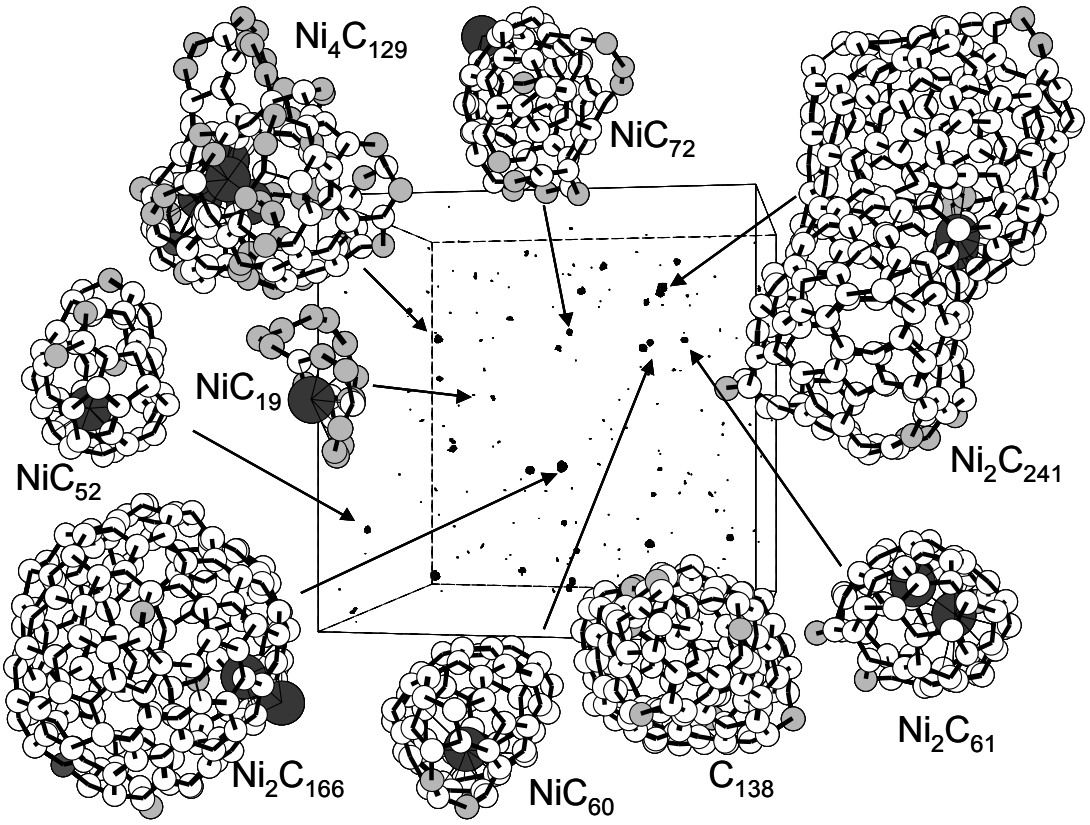

Figure 8. A snapshot of the clustering molecular dynamics simulation at 6 ns from initial random gas phase configuration. Large solid circles, empty circles, and gray circles represent Ni atoms, threehold-coordinated carbon atoms, other carbon atoms, respectively.

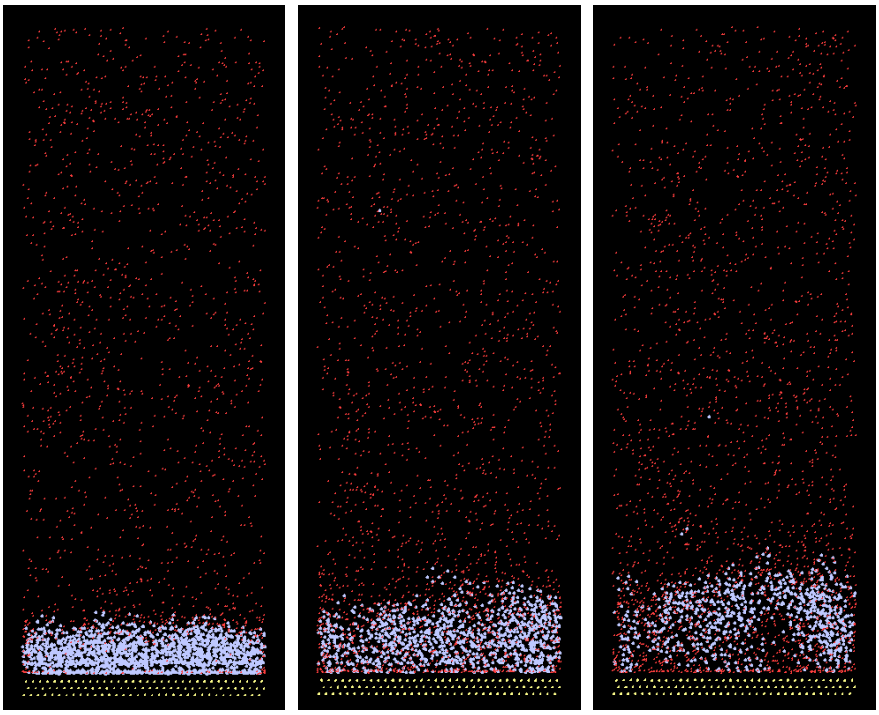

(a) 0 ps (b) 45 ps (c) 75 ps

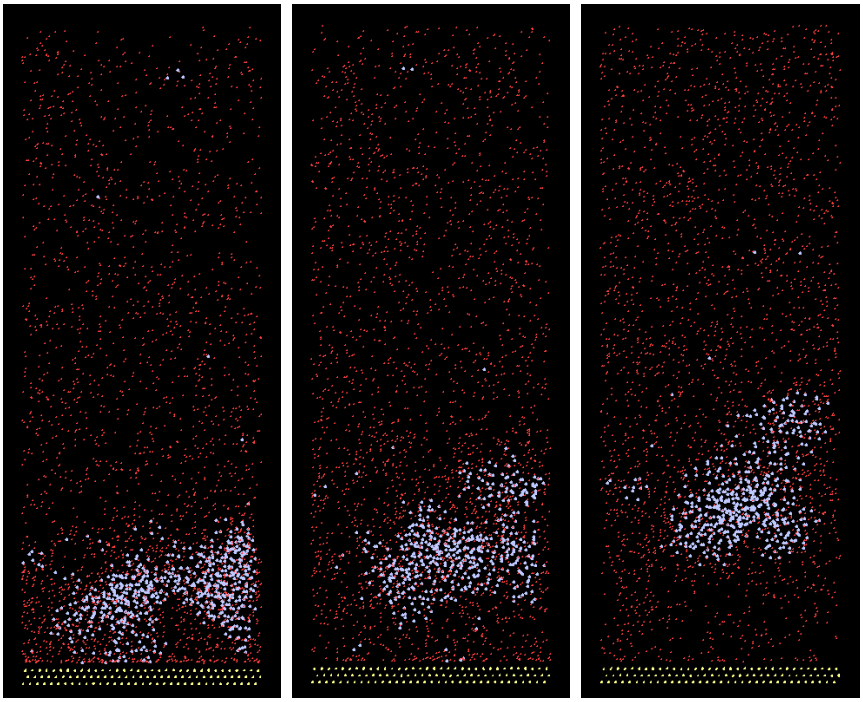

(d) 95 ps (e) 130 ps (f) 170 ps

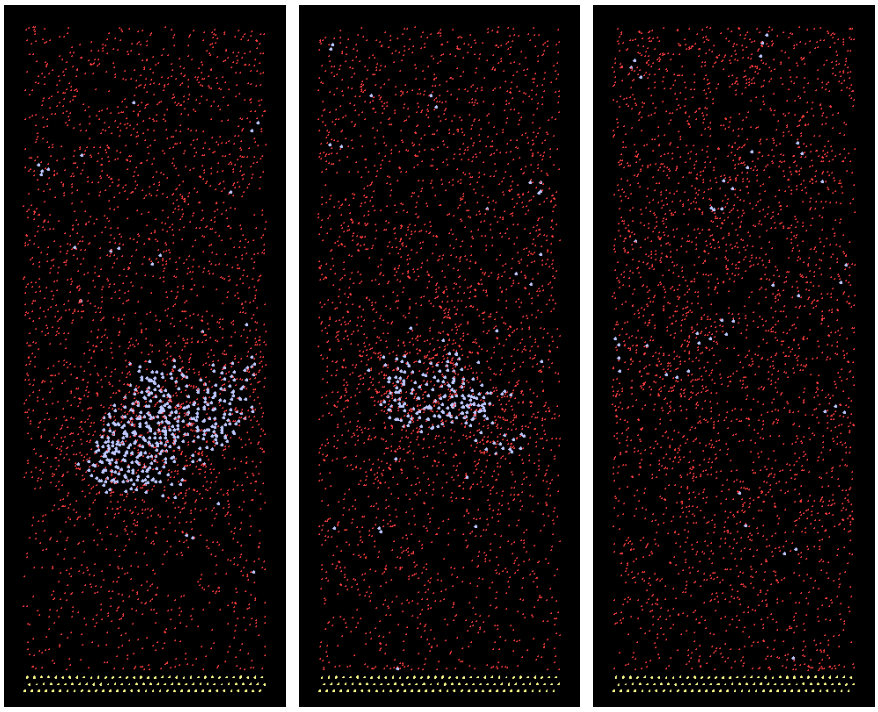

(g) 240 ps (h) 420 ps (i) 600 ps

Figure 9. Front view projection of a 3D simulation domain of an evaporating Argon layer heated from below at characteristic times — wall temperature at 300 K, [50].

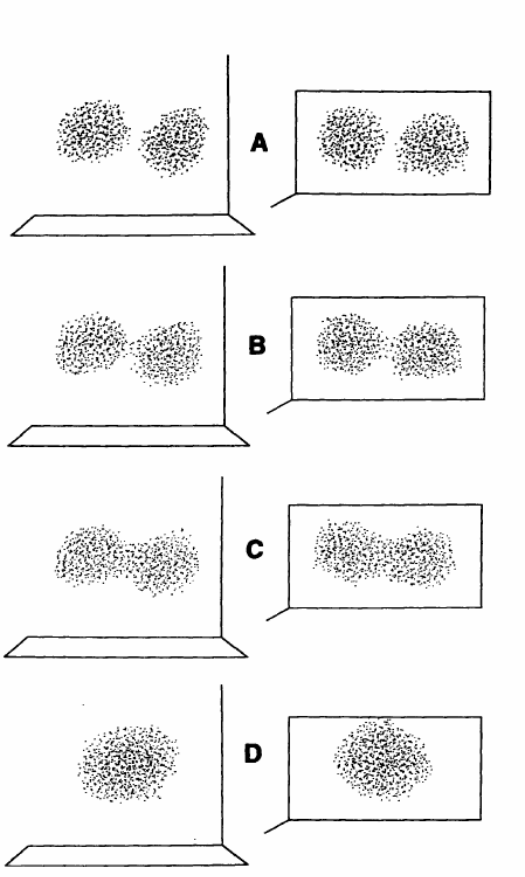

Figure 10. Drop coalescence in shear flow at different time steps, front and side view are showed, [60].

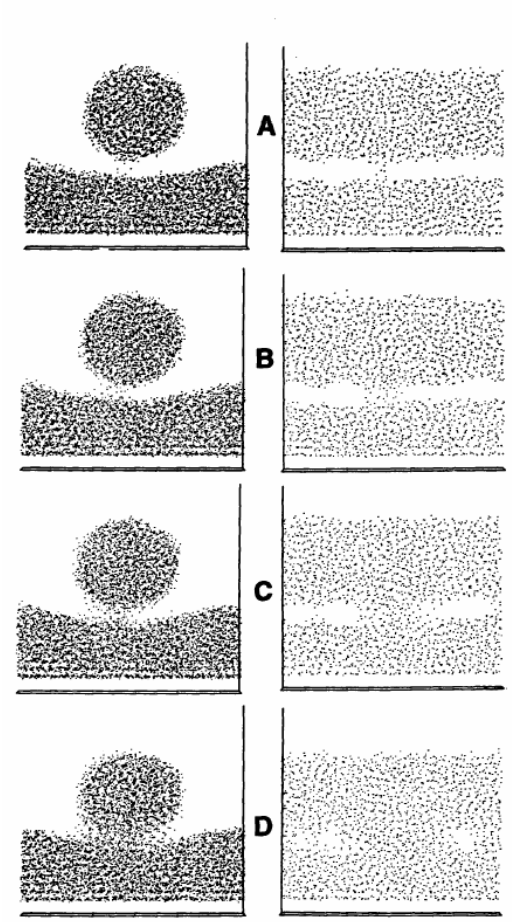

Figure 11. Coalescence of a falling liquid cylinder into a bath under gravity in an immiscible background fluid (not showed) at different instants. The side view is a cross section parallel to the cylinder axes, [60].

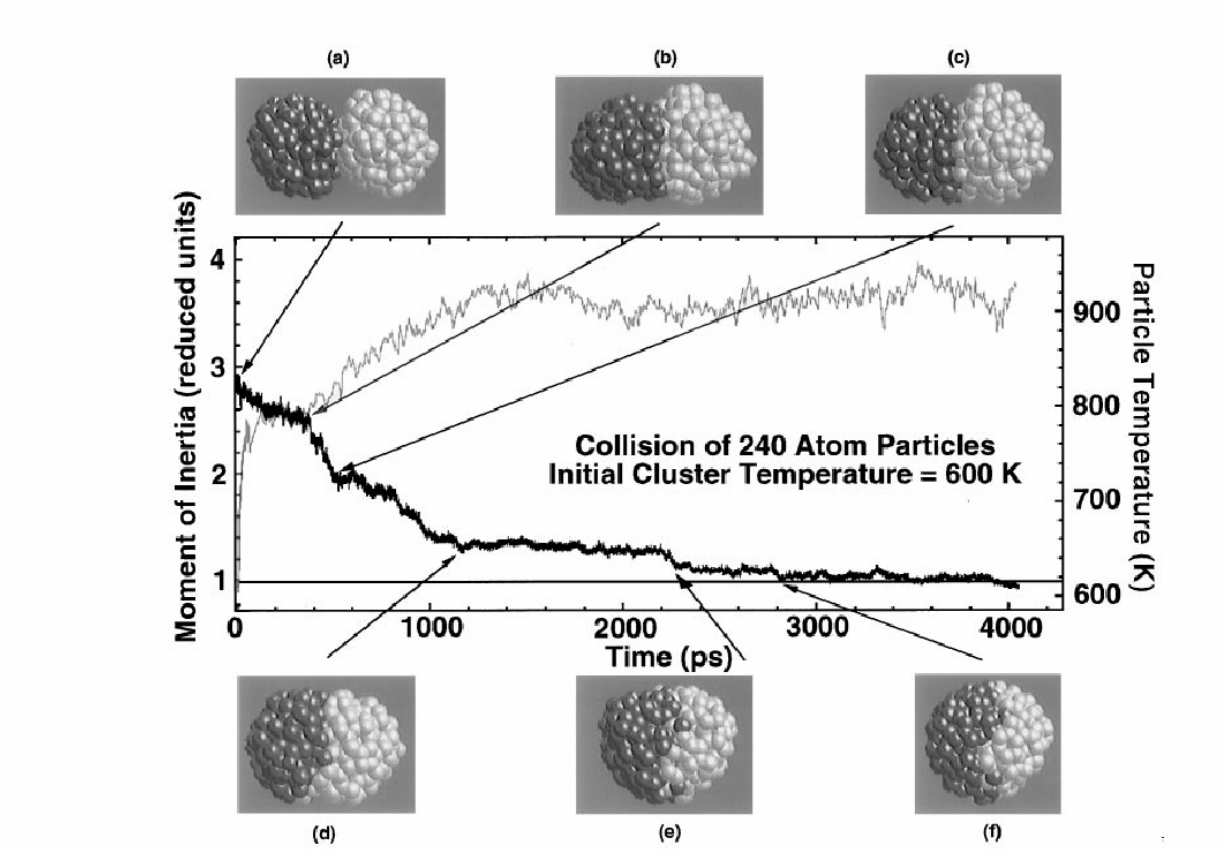

Figure 12. Temporal behavior of particle morphology as a function of temperature for the collision of two 240-atom particles, [61]. The gray curve is temperature. The black curve is the reduced moment of inertia.

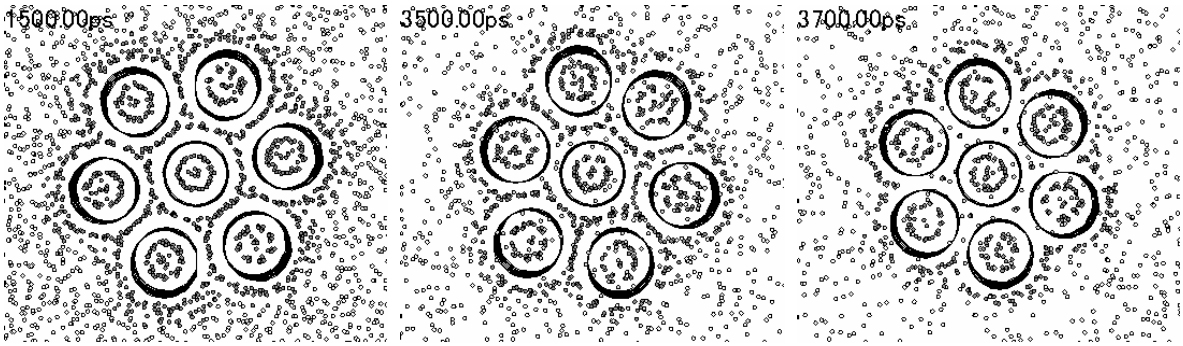

(a) (b) (c)

Figure 13. Phase transformation of a small bundle of (10.10) nanotubes with hydrogen adsorption,

[63]. Note that carbon atoms are not shown and nanotubes are shown as bonds. (a) Interstitially filled Structure; (b) Reducing Pressure to 6 Mpa;(c) Close-Packed Structure

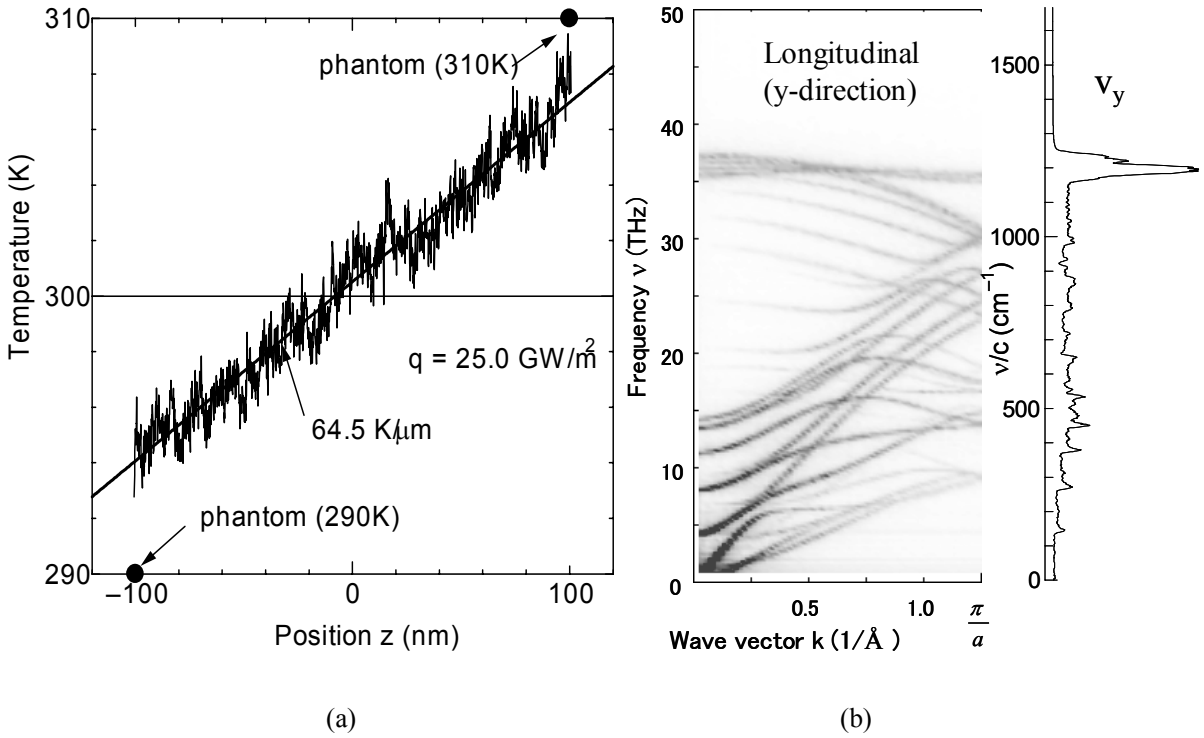

Figure 14. Molecular dynamics simulation of heat conduction along a single-walled carbon nanotube (SWNT). (a) Temperature distribution along a nanotube with (5,5) chirality and 202 nm in length. (b) Phonon dispersion relation obtained from the time-space 2-D Fourier transform of the longitudinal displacement of each molecule.